Available online at www.sciencedirect.com
ScienceDirect
Energy Conversion and Management 48 (2007) 1798–1807
ENERGY CONVERSION & MANAGEMENT
www.elsevier.com/locate/enconman

Estimating maximum sustainable injection pressure during geological sequestration of CO_2 using coupled fluid flow and geomechanical fault-slip analysis

J. Rutqvist *, J. Birkholzer, F. Cappa, C.-F. Tsang

Lawrence Berkeley National Laboratory, Earth Sciences Division, Berkeley, CA 94 720, USA

Received 26 October 2006; accepted 6 January 2007
Available online 27 March 2007

Abstract

This paper demonstrates the use of coupled fluid flow and geomechanical fault slip (fault reactivation) analysis to estimate the maximum sustainable injection pressure during geological sequestration of CO_2. Two numerical modeling approaches for analyzing fault-slip are applied, one using continuum stress–strain analysis and the other using discrete fault analysis. The results of these two approaches to numerical fault-slip analyses are compared to the results of a more conventional analytical fault-slip analysis that assumes simplified reservoir geometry. It is shown that the simplified analytical fault-slip analysis may lead to either overestimation or underestimation of the maximum sustainable injection pressure because it cannot resolve important geometrical factors associated with the injection-induced spatial evolution of fluid pressure and stress. We conclude that a fully coupled numerical analysis can more accurately account for the spatial evolution of both *in situ* stresses and fluid pressure, and therefore results in a more accurate estimation of the maximum sustainable CO_2 injection pressure.

Keywords: Geological CO_2 sequestration; geomechanics; Fault slip; Stress; Caprock integrity; CO_2 injection

1. Introduction

Geological sequestration of CO_2 involves injection of supercritical CO_2 into deep-seated reservoirs overlaid by low-permeability capping formations. At an industrial CO_2 injection site, the injection rate and pressure need to be sufficiently high to inject a desired yearly mass of CO_2. The degree of overpressure (over initial reservoir pressure) that the storage reservoir can withstand is determined by the ability of its caprock to contain the injected CO_2 as a barrier of high capillarity and low permeability. The ability to contain CO_2 by capillary forces can be expressed in terms of the pressure required to displace the native caprock water, the so-called threshold pressure, which is also an important limiting factor in natural gas storage [1]. However, during CO_2 injection increasing reservoir fluid pressure will induce mechanical stresses and deformations in and around the injection formation. If the reservoir pressure becomes too large, the induced stresses may even cause irreversible mechanical changes, creating new fractures or reactivating existing faults. Such fracturing or fault reactivation could open new flow paths through otherwise high-capillarity and low-permeability capping formations and thereby substantially reduce sequestration effectiveness. The ''maximum sustainable injection pressure,'' is the maximum pressure that will not lead to such unwanted and potentially damaging effects.

In evaluating the maximum sustainable CO_2 injection pressure, much can be learned from studies related to naturally overpressured sediments and gas reservoirs [2,3]. In such formations, initiation and reactivation of brittle faults and fractures within low-permeability caprock limit the degree of overpressure. Sibson [3] concludes that reshear of existing cohesionless faults that are favorably oriented

* Corresponding author. Tel./fax: +1 510 486 5432.
E-mail address: JRutqvist@lbl.gov (J. Rutqvist).

0196-8904/$ - see front matter © 2007 Published by Elsevier Ltd.
doi:10.1016/j.enconman.2007.01.021

for frictional reactivation provides the lower limiting bound to overpressures, whereas drainage of conduits by hydraulic extension fracturing is important only in the case of intact caprock under low-differential stress. In fractured rocks, it has also been observed that fractures favorably oriented for slip, so-called critically stressed fractures, tend to be active ground water flow paths (e.g., [4]). If shear slip occurs on a critically stressed fracture, it can raise the permeability of the fracture through several mechanisms, including brecciation, surface roughness, and breakdown of seals [4]. Given the role of fault reactivation and fracturing in naturally overpressured reservoirs and other types of fractured rock, the potential for fault reactivation must be seen as a key issue in the design and performance assessment of industrial CO_2 sequestration sites.

In this paper, we describe and demonstrate the application of coupled fluid flow and geomechanical fault-slip (fault reactivation) analysis for estimating maximum sustainable injection pressure at a CO_2 sequestration site. In Section 2, we first describe "conventional" analytic fault-reactivation-analysis techniques, and then in Section 3, we describe our numerical modeling approach. In Section 4, the maximum sustainable injection pressure is studied for two modeling approaches, one involving continuum stress–strain analysis and the other using discrete fault analysis. The results of maximum sustainable pressure for the two modeling approaches are also compared to that of simplified analytical estimates. Finally, we provide a discussion and concluding remarks related to determination of maximum sustainable injection pressure for geological CO_2 storage operations.

2. Analytical shear-slip analysis

Analytical techniques for studying shear slip along faults (fault reactivation) were originally developed and applied to study earthquakes and effects of fault reactivation on hydrocarbon accumulations. Recently, these techniques have also been applied to the study of fault stability associated with CO_2 sequestration (e.g., [5]). Analytical shear-slip analysis is conducted using principal stress magnitudes and orientations with respect to pre-existing fault planes and fluid pressure within the fault plane [5,6] (Fig. 1a). The most fundamental criterion for fault (shear) slip is derived from the effective stress law and the Coulomb criterion, rewritten as

$$\tau = C + \mu(\sigma_n - p) \quad (1)$$

where τ is shear stress, C is cohesion, μ is coefficient of friction, σ_n is normal stress, and p is fluid pressure [7]. The shear and normal stress across the plane can be calculated from the two-dimensional normal and shear stresses as (Fig. 1a)

$$\tau = \frac{1}{2}(\sigma_z - \sigma_x)\sin 2\theta + \tau_{xz}\cos 2\theta \quad (2)$$

$$\sigma_n = \sigma_x \cos^2\theta + \sigma_z \sin^2\theta + 2\tau_{xz}\cos 2\theta \quad (3)$$

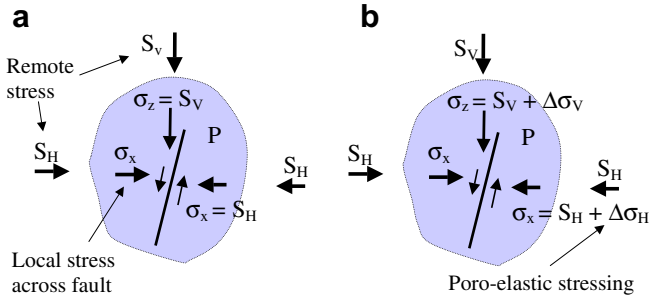

Fig. 1. Schematic of *in situ* stresses and fluid pressure considered in fault reactivation analysis. (a) Simplifying assumption in which local stresses are equal to pre-injection and remote stresses and (b) local stresses are the sum of remote and injection-induced poro-elastic stress. S_H and S_V are remote (and initial) horizontal and vertical stresses, respectively.

Eq. (1) indicates that increasing fluid pressure during an underground injection (for example) may induce shear slip (Fig. 2a).

Analytical shear-slip analysis usually aims at determining where and when (at what fluid pressure) fault reactivation may occur, and what mode of reactivation (e.g., reverse, normal, or strike-slip fault reactivation) is most likely. The results may be presented in three-dimensional contour plots and stereographic projection plots, indicating locations and orientations of faults that are most prone to slip—e.g., [5,8].

Fault stability is frequently evaluated in terms of the ratio of shear stress to effective normal stress (τ/σ_n') acting on the fault plane [5,9]. This ratio is sometimes called the "slip tendency" or "ambient stress ratio" [9]. According to Eq. (1), for a cohesionless fault ($C = 0$), slip will be induced once the ambient stress ratio exceeds the coefficient of static friction, i.e.,

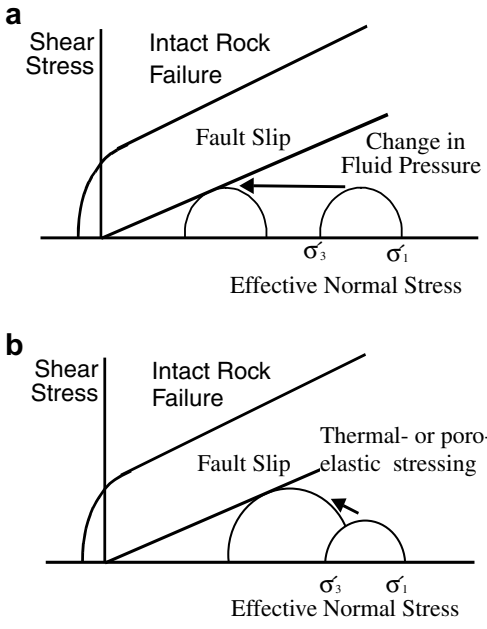

Fig. 2. Shear slip along a pre-existing fault (or fracture) as a result of (a) increased fluid pressure and (b) thermal- or poro-elastic stressing.

$$\frac{\tau}{\sigma_n - p} \geqslant \mu \tag{4}$$

where $\sigma_n - p$ is the effective normal stress, σ'_n, within the fault, i.e., $\sigma'_n = \sigma_n - P$.

The potential for fault slip may also be expressed in terms of the fluid pressure required to induce slip. The maximum sustainable injection pressure, or the critical pressure P_c, can be calculated from Eq. (1) as

$$P_c = \sigma_n - \frac{\tau}{\mu} \tag{5}$$

Comparing this P_c with a reference *in situ* pore pressure (P_p), the critical perturbation pressure (P_{cp}) can be obtained [10]. P_{cp} indicates how close a particular section of a fault is to slipping, given the reference P_p.

The coefficient of static friction, μ, is a key parameter in estimating the potential for fault slip. Field observations have shown that μ ranges approximately from 0.6 to 0.85 (e.g., [5]). Moreover, a frictional coefficient of $\mu = 0.6$ is a lower-limit value observed for the most hydraulically active fractures in fractured rock masses (e.g., [4]). Thus, using $\mu = 0.6$ in Eq. (4) would most likely give a conservative estimate of the maximum sustainable fluid pressure during a CO_2 injection, although faults containing clay minerals may have a friction coefficient less than $\mu = 0.6$ [11].

Analytical shear-slip analysis is usually based on pre-injection principal stress magnitudes and orientations corresponding to the remote stress field (Fig. 1a). However, numerical modeling, as well as observations at depleted hydrocarbon reservoirs, indicate that the *in situ* stress field may not remain constant during fluid injection, but may rather evolve in time and space, controlled by the evolutions of fluid pressure and temperature, and by site-specific structural geometry [12–14]. The stress field changes because of injection-induced poro-elastic stressing when the pressurized reservoir is prevented from expanding by the rigidity of the surrounding rock mass. As a result, the stress field acting on the fault plane changes (Fig. 1b). Such changes may in some cases lead to increased normal stress across the fault and thereby tend to prevent shear-slip. In other cases, poro-elastic stressing may change the *in situ* stress field in such a way that shear stress acting on the fault will increase and failure could be induced (Fig. 2b).

Analytical techniques may also be used to estimate the magnitude of poro-elastic stressing, albeit under simplifying geometrical assumptions. For assumed uniaxial strain conditions, representing an idealized thin, laterally extensive reservoir, under constant vertical stress, injection-induced horizontal stress may be estimated as

$$\Delta\sigma_x = \Delta P \alpha \frac{1 - 2\nu}{1 - \nu} \tag{6}$$

where α is Biot's coefficient, and ν is Poisson's ratio [13,14]. Substituting values for Biot's coefficient ($\alpha \sim 1$) and Poisson's ratio ($\nu = 0.2$–0.3), Eq. (6) indicates that $\Delta\sigma_x$ would be approximately 0.5–0.6 of ΔP. This theoretical value compares reasonably well with analyses of horizontal stress measurements in depleted hydrocarbon reservoirs [13]. The vertical stress is assumed constant and equal to the weight of the overlying rock mass because injection-induced changes in vertical stress may be small, due to the free-moving ground surface.

3. Shear-slip analysis in TOUGH-FLAC

In this section, we describe an approach to shear-slip analysis based on the coupled multiphase fluid flow and geomechanical simulator TOUGH-FLAC. The TOUGH-FLAC simulator, described in detail by Rutqvist et al. [15] and Rutqvist and Tsang [16], is based on the linking of the multiphase fluid flow simulator TOUGH2 [17] and the geomechanical code FLAC^{3D} [18]. In a coupled simulation using TOUGH-FLAC, shear-slip analysis can either be carried out as a continuum analysis or discrete fault analysis. In a continuum analysis the potential for shear slip can be evaluated by studying the time evolution of the *in situ* stresses and assessing the potential for shear slip using a failure criterion. In the case of discrete fault analysis, both extent and magnitude of shear slip can be calculated using FLAC^{3D} special fault mechanical elements.

3.1. Continuum shear-slip analysis

A continuum shear-slip analysis may be conducted using the linear elastic option of FLAC^{3D} [18]. In such a case, the coupled TOUGH-FLAC simulation calculates changes in the stress field caused by changes in pressure and temperature. The evolution of the stress field can then be compared to a failure criterion to evaluate whether shear slip is likely or not. For example, the evolution of stresses at a point may be compared to critical stresses obtained from the Coulomb criterion in Eq. (1). To evaluate the τ and σ_n needed for Eq. (1), the orientation of the fault relative to the principal stresses must be known. However, the location and orientation of fractures in the field may not be well known. It might therefore be useful, as a precaution, to assume that a fault (or pre-exiting fracture) could exist at any point with an arbitrary orientation. In such a case, the potential for shear slip can be evaluated with a Coulomb failure criterion in the following form [19]:

$$|\tau_{m2}| = (\sigma_{m2} - P_c)\sin\varphi + S_0\cos\varphi \tag{7}$$

where τ_{m2} and σ_{m2} are the two-dimensional maximum shear stress and mean stress in the principal stress plane (σ_1, σ_3), defined as

$$\tau_{m2} = \frac{1}{2}(\sigma_1 - \sigma_3) \tag{8}$$

$$\sigma_{m2} = \frac{1}{2}(\sigma_1 + \sigma_3) \tag{9}$$

where S_0 and φ are the coefficient of internal cohesion and angle of internal friction of the fault, respectively.

This can also be expressed in terms of effective principal stresses as

$$\sigma_1' = C_0 + q\sigma_3' \tag{10}$$

where C_0 is the uniaxial compressive strength and q is the slope of the σ_1' versus σ_3' line, which is related to μ according to:

$$q = \left[(\mu^2 + 1)^{\frac{1}{2}} + \mu\right]^2 \tag{11}$$

The criterion in Eq. (10) will be used below, in Section 4.1 of this paper, to follow the simulated time evolution of the principal (σ_1', σ_3') stress path in relation to the principal stresses required for failure.

Note that the equations presented in this section can also be used for analytical estimates of the maximum sustainable fluid pressure. The difference in the numerical approach is that we are calculating the spatial evolution of effective stresses including site-specific geometry, whereas with the analytical techniques, we have to assume simplified geometry with uniform fluid pressure and stress distribution.

3.2. Shear-slip analysis along discrete faults

In general, the mechanical behavior of faults and fault zones can be represented in FLAC^{3D} by special mechanical interfaces (Fig. 3a), by an equivalent continuum representation using solid elements (Fig. 3b), or by a combination of mechanical interfaces and solid elements. Multiple element representation might be necessary to represent complex, heterogeneous permeability structures in major fault zones. Such a representation might include a low-permeability fault core and adjacent damaged rock zones.

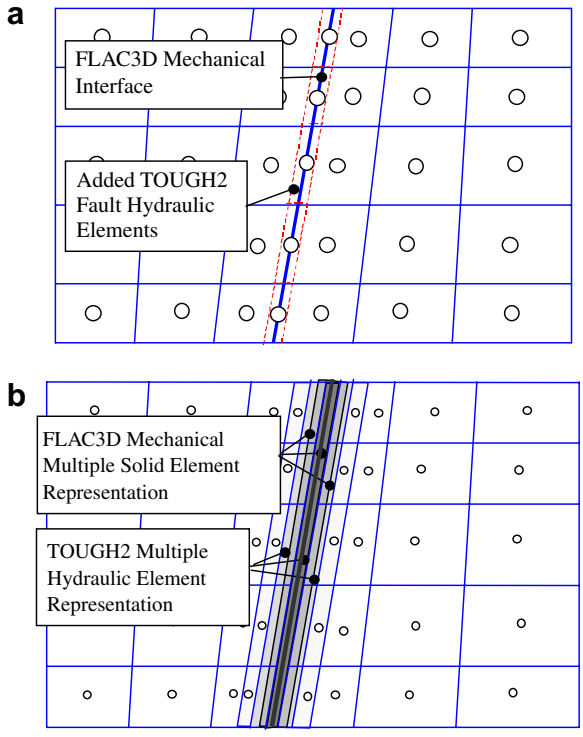

Fig. 3. Fault plane representation in coupled TOUGH2 and FLAC3D analysis using (a) FLAC3D mechanical interface, or (b) multiple solid elements with anisotropic properties.

Fig. 3a shows a fault represented by the FLAC^{3D} mechanical interface. An interface can be used to model the mechanical behavior of faults characterized by Coulomb sliding and/or separation. Interfaces have the properties of friction, cohesion, dilation, normal and shear stiffness, and tensile strength. An interface element representation is perhaps the most appropriate if the thickness of the fault is negligible compared to the size of the problem. This may include major fault zones in a regional-scale model (on the order of kilometers), or in the case of minor, single-shear fractures at a smaller scale. To simulate permeability enhancement along the interface, or sealing effects across the interface, TOUGH2 hydraulic elements must be added along the interface. The TOUGH2 hydraulic element is necessary to provide fluid pressure that will act within the fault, affecting the effective normal stress, which in turn affects the shear strength through the Coulomb criterion.

An alternative approach to the interface element is to represent the fault as an equivalent continuum using FLAC^{3D} standard solid elements (Fig. 3b). In an equivalent continuum model representation of a fault structure, the fault mechanical properties can be represented by constitutive models of various sophistication, from the simplest isotropic linear elastic to more complex elasto-plastic or visco-plastic (creep) models. One particularly useful approach, available in FLAC^{3D}, is to represent the mechanical behavior of the fault as a ubiquitously fractured media. Such a model can be used to represent strongly anisotropic mechanical behavior, including anisotropic plasticity. With anisotropic plasticity in the constitutive mechanical model, a Mohr–Coulomb shear slip behavior can be simulated, including friction, cohesion, and shear-dilation. Therefore, the mechanical behavior of the anisotropic solid element representation can be made equivalent to that of the interface element.

The use of interface elements for fault representation in TOUGH-FLAC was demonstrated by Rutqvist and Tsang [12]. However, it is generally more difficult to generate the required gridding in FLAC^{3D} and TOUGH2, and the hydromechanical coupling of FLAC^{3D} interface behavior to TOUGH2 is more complicated. Therefore, if fault mechanical behavior can be appropriately represented with solid elements, the hydromechanical coupling between FLAC^{3D} and TOUGH2 is more straightforward to implement.

4. Numerical analysis of maximum sustainable CO_2 pressure

In the next two subsections, we demonstrate the use of TOUGH-FLAC for evaluation of maximum sustainable injection pressure, using continuum shear-slip analysis and shear-slip analysis with discrete fault representation. The results of the two numerical approaches are also com-

pared to simplified analytical estimates of maximum sustainable injection pressure. The fluid properties are calculated using the ECO2N property module in TOUGH2, which contains a comprehensive description of the thermodynamic and thermophysical properties of water–NaCl–CO_2 mixtures needed for the multiphase fluid flow analysis of CO_2 sequestration in brine water formations. The two analysis examples apply to a reservoir that has not been previously depleted and where plastic yielding does not occur.

4.1. Continuum shear-slip analysis

In this simulation example, compressed CO_2 is injected at 1500 m depth into a permeable formation overlain by low-permeability caprock (Fig. 4). Material properties and input data are given in Table 1. Some material properties, such as porosity and permeability, are actually stress-dependent according to details given in [12]. However, the stress-dependent effects are not relevant for the analysis presented in this paper, where we focus on the potential for fault reactivation.

In this analysis, the potential for shear slip is estimated by substituting zero cohesion ($S_0 = 0 \Rightarrow C_0 = 0$) and a friction angle of 30° into Eq. (10), leading to the following criterion for shear slip:

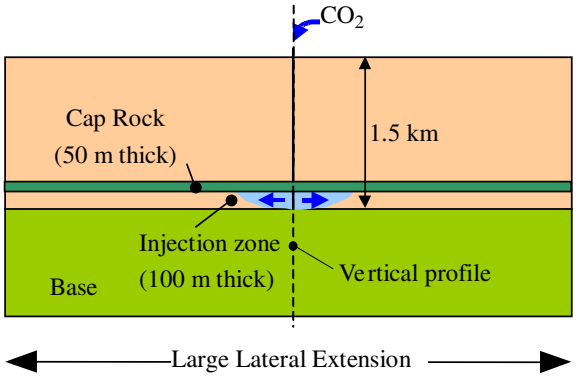

Fig. 4. Schematic of model geometry for modeling of CO_2 injection and continuum shear-slip.

$$\sigma'_1 = 3\sigma'_3 \tag{12}$$

where $3\sigma'_3$ is equal to the critical maximum principal effective stress σ'_{1c}. Thus, shear slip would be induced whenever the maximum principal effective stress exceeds three times the minimum compressive effective stress.

Zero cohesion and a friction angle of 30° correspond to a static coefficient of friction $\mu_s = \tan 30° \approx 0.6$, which is, as mentioned in Section 2, a lower-limit value frequently observed in studies of the correlation between hydraulic conducting fractures and maximum shear stress in fractured rock masses [4]. We simulate a constant-rate CO_2 injection, evaluating the maximum sustainable injection pressure for two different stress regimes: (1) a compressional stress regime with $S_H = 1.5 \times S_V$, and (2) an extensional stress regime with $S_H = 0.7 \times S_V$, where S_H and S_V are remote (and initial) horizontal and vertical stresses, respectively.

4.1.1. Numerical simulation results

Figs. 5 and 6 presents the numerical simulation results in terms of the vertical profiles of several key parameters after 3 years of injection. At this time, the injection pressure has reached 27 MPa, which is about 80% of the lithostatic stress (Fig. 5a) and the CO_2 is completely contained within the injection zone (Fig. 5b). However, the increased fluid pressure within the injection zone and the overlying caprock induces changes in horizontal and vertical effective stresses, according to:

$$\Delta\sigma'_x = \Delta\sigma_x - \Delta P \tag{13}$$

$$\Delta\sigma'_z = \Delta\sigma_z - \Delta P \tag{14}$$

Fig. 5c and d shows that both effective and total (confining) stresses change with the changed reservoir pressure. Increases in total stresses are caused by poro-elastic expansion, which is partly restricted by the stiffness of the surrounding rock-mass structure. In general, effective stress changes much more in the vertical direction, as a result of the free-moving ground surface [12].

Changes in the stress field shown in Fig. 5c and d should be added to the initial pre-injection *in situ* stresses to obtain the stress field after 3 years of injection. However, the three-dimensional pre-injection *in situ* stress field may not

Table 1
Material properties used in TOUGH-FLAC simulations

Property	Upper	Cap	Aquifer	Basement
Young's modulus, E (GPa)	5	5	5	5
Poisson's ratio, ν (–)	0.25	0.25	0.25	0.25
Biot's parameter, α (–)	1	1	1	1
Saturated rock density, ρ_s (kg/m^3)	2260	2260	2260	2260
Porosity, ϕ (–)	0.1	0.01	0.1	0.01
Permeability, k (m^2)	1×10^{-15}	1×10^{-17}	1×10^{-13}	1×10^{-17}
Corey [20] irreducible gas saturation, S_{rg} (–)	0.05	0.05	0.05	0.05
Corey [20] irreducible liquid saturation, S_{rl}	0.3	0.3	0.3	0.3
van Genuchten [21] capillary strength parameter, P (kPa)	196	3100	19.6	3100
van Genuchten [21] exponent, m	0.457	0.457	0.457	0.457

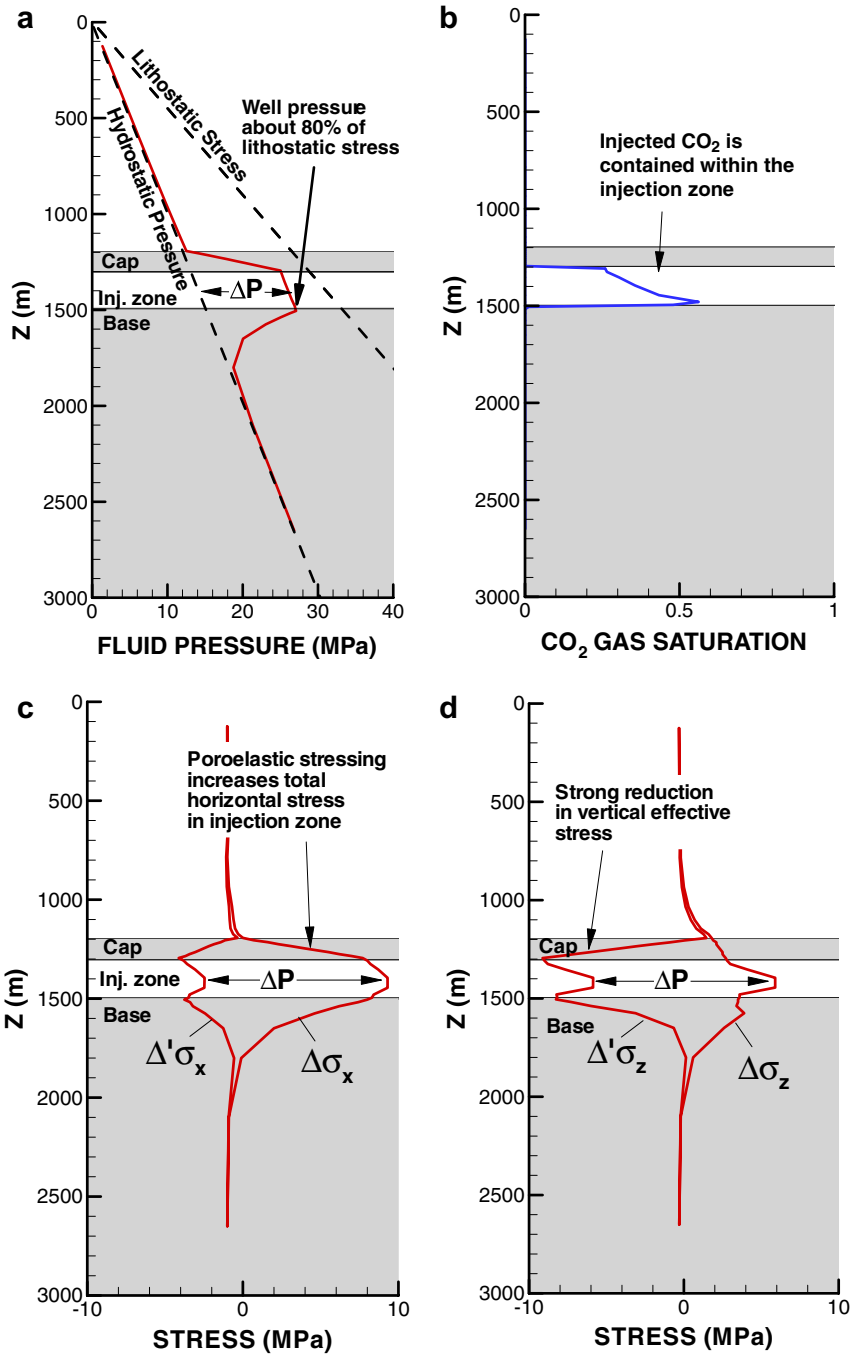

Fig. 5. Vertical profiles of (a) fluid pressure, (b) CO_2 saturation, (c) change in horizontal effective and total stress, and (d) change in vertical effective and total stress.

be entirely known. Therefore, it is useful to evaluate the maximum sustainable injection pressure for various *in situ* stress regimes, including compressional pressure regime (for which $S_H > S_V$) and extensional regime (for which $S_H < S_V$).

Fig. 6a and b presents vertical profiles for evaluation of shear-slip potential for the two different stress regimes. In the case of a compressional stress regime (Fig. 6a), shear slip is most likely in the lower part of the cap, at the interface with the injection zone, and at the lower part of the injection zone. However, the shear slip would probably not propagate through the upper part of the cap, which would thus remain intact. In the case of an extensional stress regime (Fig. 6b), shear slip might first be induced near the ground surface and in the overburden rock above the zone of pressure increase. Thereafter, shear slip might also be induced in the caprock, just above the injection zone.

In Fig. 7, the path of the principal effective stresses, σ'_1 and σ'_3, in the lower part of the caprock (near its interface with the injection zone) is plotted and compared to the failure criterion in Eq. (12). For a compressional stress field,

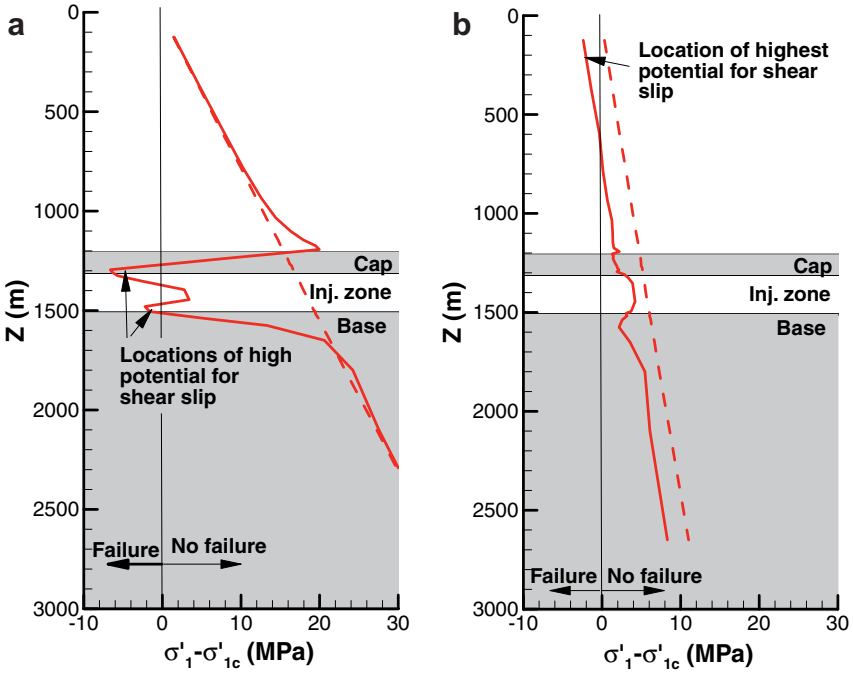

Fig. 6. Vertical profiles of $\sigma'_1 - \sigma'_{1c} = \sigma'_1 - 3\sigma'_3$ for (a) compressional and (b) extensional stress regimes.

the principal stresses would move into a region of likely shear slip after just over one year of injection at an injection pressure of about 24 MPa. In an extensional stress regime, shear slip could occur just after three years of injection at an injection pressure of about 28 MPa.

4.1.2. Comparison to simplified analytical estimates

The maximum sustainable injection pressure may be estimated analytically using Eq. (12) for lithostatic vertical stress, $S_V = 33.2$ MPa, at 1500 m, and with different horizontal stress, $S_H = 1.5S_V$ or $S_H = 0.7S_V$, depending on the assumed stress regime. The critical pressure P_c for inducing shear slip on an arbitrarily oriented fault can be derived from Eq. (12) by considering that shear slip occurs when $P = P_c$, that is we insert $\sigma'_1 = \sigma_1 - P_c$ and $\sigma'_3 = \sigma_3 - P_c$ into Eq. (12)

$$P_c = \frac{3\sigma_3 - \sigma_1}{2} \tag{15}$$

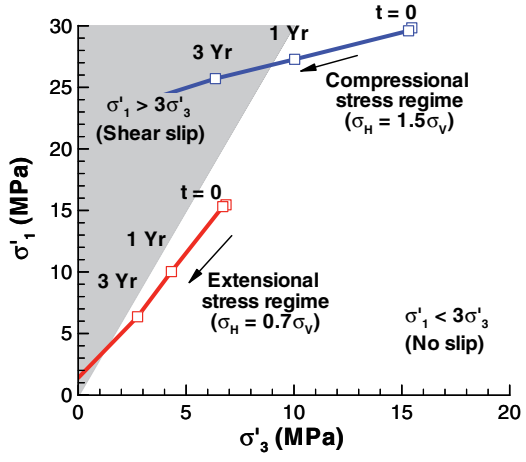

Fig. 7. Principal (effective) stress path at the bottom of the caprock for compressional and extensional stress regimes.

First, estimating the maximum sustainable injection pressure from the initial (pre-injection) stress field, we assume that the local stresses are equal to the remote stresses, i.e. $\sigma_y = S_V$ and $\sigma_x = S_H$ (Fig. 1a). For a compressional stress regime, $\sigma_1 = \sigma_x = S_H = 1.5S_V = 49.8$ MPa and $\sigma_3 = \sigma_y = S_V = 33.2$ MPa, whereas for an extensional stress regime, $\sigma_1 = \sigma_y = S_V = 33.2$ MPa and $\sigma_3 = \sigma_x = S_H = 0.7S_V = 23.2$ MPa. By substituting these numbers into Eq. (15), the simplified analytical estimate of the maximum sustainable injection pressure is 25 MPa for a compressional stress regime and 18 MPa for an extensional stress regime. These numbers indicate that the simplified analytical estimate excluding poro-elastic stress is similar to that of the numerical analysis for a compressional stress regime, whereas the simplified estimate for an extensional stress regime is overly conservative—that is, the maximum sustainable injection pressure is underestimated (see Table 2). For the extensional stress regime, the maximum sustainable injection pressure is underestimated by Eq. (15) because it neglects injection-induced poro-elastic stressing that tends to increase the minimum principal stress, which in this case is horizontal.

If we consider the poro-elastic stressing analytically, using Eq. (6) and a Poisson's ratio of 0.25 (Table 1), we find that $\Delta\sigma_x = 2\Delta P/3 \approx 0.67\Delta P$. In this case the local horizontal stresses should be calculated as $\sigma_x = S_H +$

Table 2
Comparison of numerical results with simplified analytical results of maximum sustainable injection pressure in the continuum analysis case

Stress regime	Maximum sustainable injection pressure (MPa)		
	Numerical simulation results	Simplified analytical estimate using pre-injection stress	Simplified analytical estimate including estimate of poro-elastic stress
Compressional ($S_h = 1.5S_v$)	24	25	27
Extensional ($S_h = 0.7S_v$)	28	18	63

$\Delta\sigma_x = S_H + 2\Delta P/3$ (see also Fig. 1b). Thus, for a compressional stress regime, $\sigma_1 = \sigma_x = S_H + 2\Delta P/3 = 1.5S_V + 2\Delta P/3$ and $\sigma_3 = \sigma_y = S_V$. For the extensional stress regime, $\sigma_1 = \sigma_y = S_v$ and $\sigma_3 = \sigma_x = S_H + 2\Delta P/3 = 0.7S_V + 2\Delta P/3$, if $\Delta P < 15$ MPa (if ΔP exceeds 15 MPa, the maximum principal compressive stress becomes horizontal). By substituting these parameters into Eq. (15), we determined a critical pressure $P_c = 27.2$ MPa for a compressional stress regime. For an extensional stress regime, the solution with the above parameters indicates that a critical pressure will never be reached, but the estimated poro-elastic stress becomes very high and shifts the maximum principal stress from vertical to horizontal, resulting in a very high critical pressure ($P_c \approx 63$ MPa). Thus, for an extensional stress regime, the simplified analytical estimate including poro-elastic stress grossly overestimates the maximum sustainable injection pressure (Table 2).

4.2. Shear-slip analysis with a discrete fault

In this simulation example, a shear-slip analysis is conducted using a discrete fault representation in TOUGH-FLAC. As in the previous example, compressed CO_2 is injected at 1500 m depth into a permeable formation overlain by a low-permeability caprock. However, in this case, the injection zone is effectively bounded by an offset fault (Fig. 8). In this example, an extensional stress regime with $S_H = 0.7 \times S_V$ is assumed, and the fault is considered cohesionless, with a friction angle of 25°.

4.2.1. Numerical simulation results

In the TOUGH-FLAC simulation, the fault is discretized into solid elements with anisotropy of mechanical (elasto-plastic) and hydrologic properties. In this model, fault permeability changes with shear such that for a fully reactivated fault (maximum shear strain), permeability increases by two orders of magnitude. This is simulated by relating the permeability changes, k/k_0, to maximum shear strain, ε_{sh}, according to:

$$\frac{k}{k_0} = 1 + \beta \cdot \Delta\varepsilon_{sh} \quad (16)$$

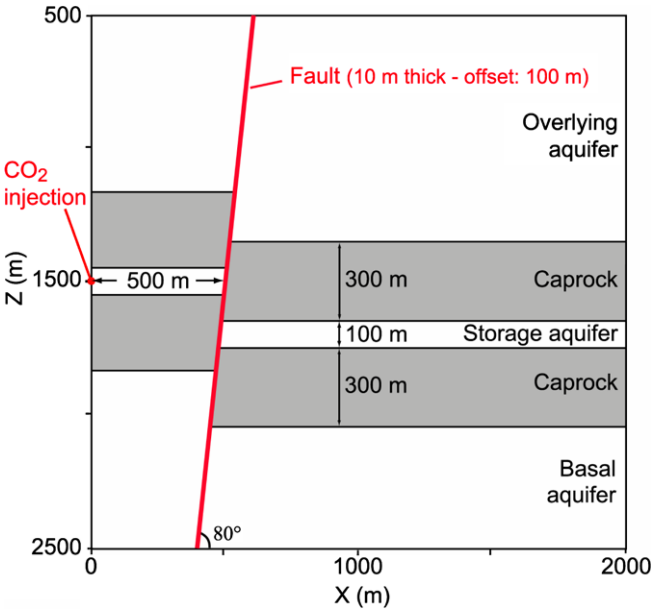

Fig. 8. Schematic for TOUGH-FLAC modeling of discrete fault hydro-mechanical behavior during CO_2 injection.

where β is set to 1×10^{-4} to obtain a two-order-of-magnitude permeability increase for a fully reactivated fault. Other material properties and input data are similar to that of the above continuum shear-slip analysis (Table 1).

Fig. 9 shows the evolution of injection pressure during the constant-rate CO_2 injection, whereas Figs. 10 and 11 shows contour plots that can help to explain the pressure responses in Fig. 9. In Fig. 9, the fully coupled hydromechanical simulation (solid line in Fig. 9) is compared to an uncoupled simulation with no fault reactivation (dashed line in Fig. 9). If no fault reactivation is considered, fluid pressure would quickly rise above lithostatic stress. On the other hand, if fault reactivation and shear-induced permeability changes are considered, the injection pressure does not rise as high, but peaks at a magnitude well below lithostatic stress. Fig. 10 shows that after 6 months, the zone of shear slip, observed as a zone of localized substantial shear strain, extends all the way through the upper cap.

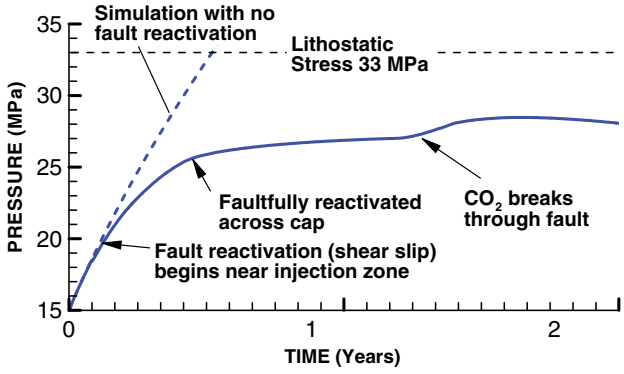

Fig. 9. Simulated evolution of injection pressure with and without consideration of shear-slip-induced fault permeability changes.

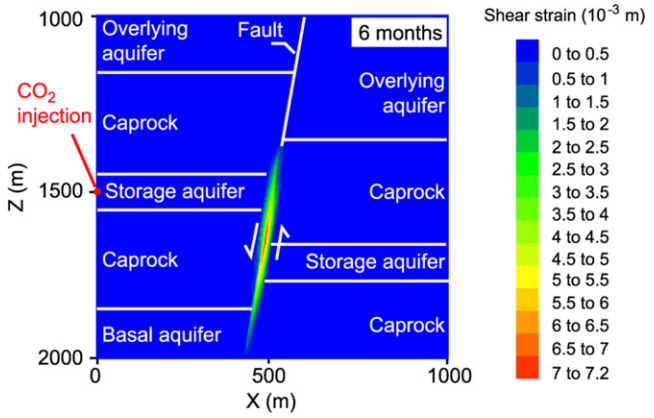

Fig. 10. Contour of maximum shear strain after 6 months of injection.

Thus, a new flow path has opened up across the upper cap. As a result, reservoir pressure can be released through the fault once it has opened all the way. Moreover, after about 1 year and 4 months, the injected CO_2-rich fluid reaches and migrates up along the fault (see spread of CO_2 at 1 and 3 years Fig. 11).

From Fig. 9, the maximum sustainable injection pressure might be estimated to be in the range of 19–25 MPa. The first sign of shear-induced permeability change occurs after about 1.5 months at an injection pressure of about 19 MPa. This finding indicates some shear slip and permeability change, but shear slip does not propagate across the upper cap until the injection pressure reaches about 25 MPa, which occurs after about 6 months of injection. Actually, at 19 MPa, the injection pressure is affected by leakage into the underlying formation. Upward leakage to overlying formations does not occur until the fault slip has propagated through the upper cap, which occurs after 6 months at an injection pressure of about 25 MPa. Therefore, the maximum sustainable injection pressure estimated to be 25 MPa.

4.2.2. Comparison to simplified analytical estimates

In this case we can also estimate the maximum sustainable injection pressure using Eq. (1), for the undisturbed initial stress field. At the depth of injection, the initial stresses are $S_V = 33$ MPa, and $S_H = 0.7 \times S_V = 23$ MPa. Using Eq. (1) and considering the fault angle for estimation of τ and σ_n, we estimate the maximum sustainable injection pressure to be $P_c \approx 20$ MPa. If we also consider an analytical estimate of injection-induced poro-elastic stress change by $\Delta\sigma_x = 2\Delta P/3 \approx 0.67\Delta P$ (see Section 4.1), the maximum sustainable injection pressure is estimated to be $P_c \approx 43$ MPa. Because the numerical modeling results resulted in a maximum sustainable injection pressure of 25 MPa, the simplified analytical estimate either underestimates or overestimates by a wide margin the maximum sustainable injection pressure (see also Table 3).

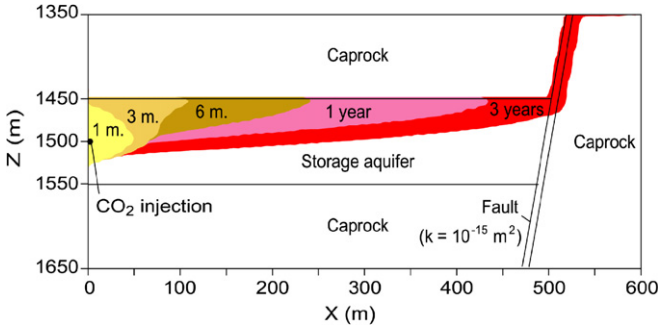

Fig. 11. Simulated evolution of CO_2-rich phase. The contours indicates how far the CO_2-rich fluid have spread as a separate phase after 1 month, 3 months, 6 months, 1 year and 3 years of injection.

Table 3
Comparison of numerical results with simplified analytical results of maximum sustainable injection pressure in the discrete fault case

Maximum sustainable injection pressure (MPa)		
Numerical simulation results	Simplified analytical estimate using pre-injection stress	Simplified analytical estimate including estimate of poro-elastic stress
25	20	43

5. Discussion

Our analysis indicates that simplified analytical techniques may either underestimate or overestimate the maximum sustainable injection pressure. The main reason is that analytical techniques require simplifying assumptions regarding geometry and distribution of pressure and stress. The poro-elastic effects seem to be particularly difficult to estimate, since their distribution can be very different in the reservoir center than in the overlying caprock. Therefore, the simplified analytical techniques described in Section 2 should perhaps be used as an initial first-order estimate of the potential for shear slip and for identification of the most critically oriented faults in a geological system. On the other hand, a coupled numerical analysis such as that provided by TOUGH-FLAC has the potential to evaluate the injection-induced spatial evolution of both fluid pressure and stress, including important mechanical interactions between the reservoir rock and overlying caprock. Moreover, using coupled fluid flow and geomechanical numerical modeling, the shear-slip analysis can be fully integrated with the multiphase fluid flow reservoir analysis of a site and can therefore be used for design and optimization of injection/withdrawal operations. Such optimization could include maximizing injected CO_2 mass while minimizing the risk for leakage.

6. Concluding remarks

In this paper, we describe and demonstrate the use of coupled multiphase fluid flow and geomechanical fault-slip analysis for estimation of maximum sustainable injection pressure during geological sequestration of CO_2. Comparison of numerical results to that of analytical estimates

using simplifying geometrical assumptions showed that the simplified analytical estimates might either overestimate or underestimate the maximum sustainable injection pressure. When conventional analytical techniques are used without accounting for poro-elastic stresses, the analytical estimates are in most cases going to be conservative. If poro-elastic stressing is considered in the analytical estimates using the assumption of uniaxial strain conditions, the maximum sustainable injection pressure might be grossly overestimated. The main advantage of the numerical approach presented in this paper (compared to more conventional simplified analytical methods) is that the coupled numerical analysis more accurately takes into account structural geometry and its effect on the injection-induced spatial evolution of fluid pressure and *in situ* stress. Therefore, the numerical analysis results in a more accurate estimation of the maximum sustainable CO_2 injection pressure.

Acknowledgements

The work presented in this paper was financed by contributions from the Ministry of Economy, Trade and Industry Ministry (METI) of Japan, and the US Environmental Protection Agency, Office of Water and Office of Air and Radiation, under an Interagency Agreement with the US Department of Energy at the Lawrence Berkeley National Laboratory, No. DE-AC02-05CH11231.

References

[1] Thomas LK, Katz DL, Tek MR. Threshold pressure phenomena in porous media. Soc Petrol Eng J 1968(June):174–84.
[2] Poston SW, Berg RR. Overpressured gas reservoirs. Richardson (TX): Society of Petroleum Engineers; 1997. p. 138.
[3] Sibson RH. Brittle-failure controls on maximum sustainable overpressure in different tectonic stress regimes. Bull Am Assoc Petrol Geol 2003;87:901–8.
[4] Barton CA, Zoback MD, Moos D. Fluid flow along potentially active faults in crystalline rock. Geology 1995;23:683–6.
[5] Streit JE, Hillis RR. Estimating fault stability and sustainable fluid pressures for underground storage of CO_2 in porous rock. Energy 2004;29:1445–56.
[6] Wiprut D, Zoback MD. Fault reactivation and fluid flow along a previously dormant normal fault in the northern North Sea. Geology 2000;28:595–8.
[7] Scholz CH. The mechanics of earthquakes and faulting. New York: Cambridge University Press; 1990.
[8] van Ruth PJ, Nelson E, Hillis RR. Fault reactivation potential during CO_2 injection in the Gippsland Basin, Australia. Explor Geophys 2006;37:50–6.
[9] Morris A, Ferril DA, Henderson DB. Slip tendency analysis and fault reactivation. Geology 1996;24:275–8.
[10] Chiaramonte L, Zoback M, Friedmann J, Stamp V. CO_2 sequestration, fault stability and seal integrity at Teapot Dome, Wyoming. In: 8th International conference on greenhouse gas control technologies, Trondheim, Norway, June 19–22, 2006.
[11] Byerlee J. Friction of rocks. Pure Appl Geophys 1978;116:615–26.
[12] Rutqvist J, Tsang C-F. Coupled hydromechanical effects of CO_2 injection. In: Tsang CF, Apps JA, editors. Injection science and technology. Elsevier; 2005. p. 649–79.
[13] Hawkes CD, McLellan PJ, Zimmer U, Bachu S. Geomechanical factors affecting geological storage of CO_2 in depleted oil and gas reservoirs: risks and mechanisms. In: Proceedings of Gulf Rocks 2004, the 6th North America Rock Mechanics Symposium (NARMS): Rock Mechanics Across Borders and Disciplines, Houston, Texas, June 5–9, 2004.
[14] Hillis RR. Coupled changes in pore pressure and stress in oil fields and sedimentary basins. Petrol Geosci 2001;7:419–25.
[15] Rutqvist J, Wu YS, Tsang C-F, Bodvarsson G. A modeling approach for analysis of coupled multiphase fluid flow, heat transfer, and deformation in fractured porous rock. Int J Rock Mech Min Sci 2002;39:429–42.
[16] Rutqvist J, Tsang C-F. TOUGH-FLAC: a numerical simulator for analysis of coupled thermal-hydrologic-mechanical processes in fractured and porous geological media under multi-phase flow conditions. Proceedings of the TOUGH symposium. Berkeley: Lawrence Berkeley National Laboratory; 2003. May 12–14.
[17] Pruess K, Oldenburg C, and Moridis G. TOUGH2 User's Guide, Version 2.0, Report LBNL-43134, Lawrence Berkeley National Laboratory, Berkeley (CA), 1999.
[18] Itasca Consulting Group, FLAC 3D, Fast Lagrangian analysis of continua in 3 dimensions. Version 2.0. Five volumes. Minneapolis, Minnesota, Itasca Consulting Group, 1997.
[19] Jaeger JC, Cook NGW. Fundamentals of rock mechanics. London: Chapman and Hall; 1979. p. 593.
[20] Corey AT. The interrelation between oil and gas relative permeabilities. Prod Monthly 1954(November):38–41.
[21] van Genuchten MT. A closed-form equation for predicting the hydraulic conductivity of unsaturated soils. Soil Sci Soc Am J 1980;44:892–8.